Proceedings of the ASME 2022
Fluids Engineering Division Summer Meeting
FEDSM2022
August 3-5, 2022, Toronto, Ontario, Canada

FEDSM2022-88368

AERODYNAMIC ANALYSIS OF THE UTILITY TRUCK WITH THE MORPHING BOOM EQUIPMENT

Parth Y. Patel[1], Thannathorn Jannoi[1], Wenhui Zou[1], Vladimir Vantsevich[1], and Roy Koomullil[1]
University of Alabama at Birmingham
Birmingham, AL

ABSTRACT

Global climate change has affected the human race for decades. As a result, severe weather changes and more substantial hurricane impact have become a typical scenario. Utility trucks with the morphing boom equipment are the first responders to access these disaster areas in bad weather conditions and restore the damages caused by the disaster. The stability of the utility trucks while driving in a heavy wind scenario is an essential aspect for the safety of the rescue crew, and aerodynamic forces caused by the wind flow constitute a significant factor that influences the stability of the utility truck. In this paper, the aerodynamic performance of the utility truck is modeled using the incompressible unsteady Reynolds Averaged Navier Stokes (URANS) model. The Ahmed body, a well-recognized benchmark test case used by the computational fluid dynamics (CFD) community for the aerodynamic model validation of automobiles, is used to validate this aerodynamic model. The validated aerodynamic model investigates the impact of heavy wind on the utility truck with the morphing boom equipment. The visualization of the flow field around the utility truck with the force and moment coefficients at various side slip angles are presented in this paper.

Keywords: Utility Truck, CFD Aerodynamic Simulations, Ahmed Body, Morphing Boom Equipment.

NOMENCLATURE

ρ	density of air (kg/m^3)
μ	dynamic viscosity (Pa-s)
δ	delta function (unit varies)
p	pressure (Pa)
k	kinetic energy per unit mass (J/kg)
ω	specific dissipation rate (s^{-1})
α	side slip angle (degree)
S	strain rate magnitude
A	frontal area of the truck (m^2)
V	total velocity of vehicle speed and wind speed (m/s)
L	reference length (m)

1. INTRODUCTION

Severe weather conditions have steadily increased over the last two decades. Therefore, the safety of the rescue and repair team is of paramount importance while they attend to emergencies due to these severe weather conditions. The National Weather Service categorizes tornadoes and hurricanes based on their severity using the Fujita scale [1] and Saffir-Simpson Hurricane Wind Scale [2]. According to their categorizations, a severe weather condition generated by either tornadoes or hurricanes will have a wind speed of at least above 50 m/s, which can cause severe damages to both residents and public properties.

Utility trucks (also known as boom trucks) are the first responders in these extreme climate and weather situations from cutting trees to restoring traffic, recovering living beings from destroyed properties, repairing electric posts, and restoring power. A stable utility truck will be beneficial under this kind of situation, making the utility truck remain on the ground without skidding or even driving on the road to attend to such emergencies. According to the US Census Bureau, there are approximately 15 million trucks currently in operation across the country operated by 2.83 million drivers, 28.2% of whom drive various utility trucks [3]. Such trucks with morphing capabilities of the manipulator can increase the possibility of road accidents

in several ways and create hazardous situations on the roads and off-road conditions while moving and performing critical tasks.

When a heavy-duty truck is running at a constant speed, the air around the vehicle gets reflected, and it flows along the truck's surface, resulting in aerodynamic forces and moments of the truck. Likewise, a driving truck under the heavy crosswind is represented by the wind from the side, which causes significant changes in the aerodynamic forces and moments acting on the truck. Thus, it is essential to conduct an aerodynamic analysis to ensure the utility truck with the boom equipment is safe enough to stay on the road. A few researchers established a standard vehicle model and applied aerodynamic lateral force at the pressure center point to simulate the vehicle's stability under transient or steady crosswind. [4,5]. Several methods exist to estimate aerodynamic forces and moments, such as Computational Fluid Dynamics (CFD) to calculate the force numerically by solving the equations that govern the fluid flows, experimental measurements on a simplified model, etc. CFD is the most commonly used method to estimate aerodynamic forces. One of the advantages of this approach is the ability to change the flow conditions and conduct a parametric study quickly. For example, Dominy and Richardson [6] simulated the aerodynamic characteristics of a rally car at high slip angles with CFD simulations. Tsubokura and Nakashima [7] predicted the unsteady aerodynamic forces on a Formula car under crosswind during cornering in CFD simulations.

Aerodynamic improvements are evident to improve the heavy-duty trucks throughout the United States. As a result, aerodynamic improvements in heavy-duty trucks are becoming extremely popular, from Walmart's advanced vehicle [8] project and the Department of Energy's Super Truck [9] to more straightforward advancements such as additions to the rear of the trailer [10]. However, there is no literature available that discusses the aerodynamic behavior of utility trucks under severe weather conditions.

During the motion of the utility truck with the boom equipment, the adverse weather with the heavy cross winds seriously affects the driver's judgment, which may cause serious accidents. Therefore, an aerodynamic analysis is presented in this paper to investigate the influence of heavy wind on the utility truck's stability. An overview of the utility truck with the morphing boom equipment is provided at the beginning of the paper. One of the requirements of geometries for computational simulation is a water-tight geometry without any overlapping of the patches. Following the overview and nomenclature of the utility truck, a discussion on creating a water-tight Computer-aided design (CAD) geometry without any gaps is presented. This is followed by the numerical and physics models used in the CFD simulation are discussed. Ahmed body [11], a well-recognized benchmark test case used by the CFD community for the aerodynamic model validation of automobiles, is used to validate the aerodynamic model. the results from the validation of the aerodynamic model using the Ahmed body are presented in the section following the aerodynamic model. Finally, the aerodynamic force and moment coefficients of the F450 utility truck with morphing boom equipment obtained by CFD simulations are presented.

2. OVERVIEW OF THE UTILITY TRUCK

The utility truck is a commercial truck fitted with a hydraulic pole called the boom, which has a worker-carrying bucket at the end. This bucket helps the worker safely perform the tasks and comfortably work with the tools when the boom morphs. This eliminates the usage of scaffoldings and ladders to perform various off-the-ground tasks, which are unsafe and may lead to accidents. Figure 1 represents the configuration and component identification of the utility truck.

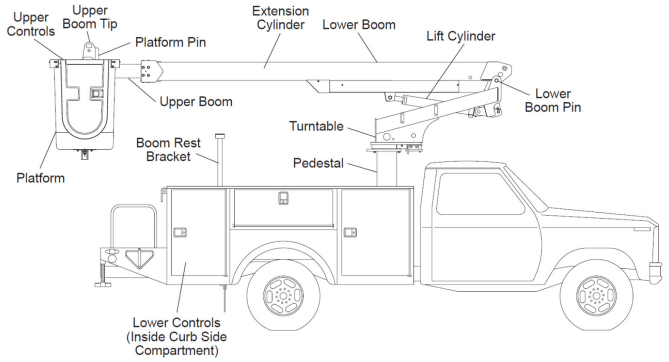

Figure 1. Configuration and component identification of the utility truck.

3. COMPUTATIONAL SIMULATION METHODOLOGY

3.1 CAD Geometry Preparation for the CFD Simulations

Cleanup and repair of complex geometries is a significant bottleneck in numerical simulations, especially in CFD simulations. Several problems in complex CAD geometry, such as small edges, sliver faces, seams, holes, and faces with sharp angles, etc., must be resolved for the computational analysis. In this regard, a water-tight solid geometry without gaps or overlaps is required for the simulations. For the needs of this research, one of the project partners, Altec Inc. [12], provided a complex CAD geometry model in SolidWorks format of an F450 utility truck with the boom equipment as shown in Figures 2 and 3. This geometry was defined using over 800 components and many of these components were inside of the truck, which are irrelevant for CFD simulations. As demonstrated from Figures 2 and 3, this geometry has several overlapping surfaces, gaps, missing faces, and the presence of many details that are irrelevant for the CFD simulations.

Simplification of the geometry was done by removing some of the superfluous parts that do not affect the aerodynamic analysis of the truck such as the chassis, exhausting pipe, stairs, axels, searching lights, control panel, tag holders, rear lights, draw handlers, hookers, mud covers etc. to make the geometry as a solid object with flat surfaces. After simplifying the geometry in SolidWorks [13], we imported it into the ANSYS

SpaceClaim [14] for further simplification, as shown in Figure 4.

Figure 2. Isometric View: Complex CAD geometry of the utility truck with the boom equipment

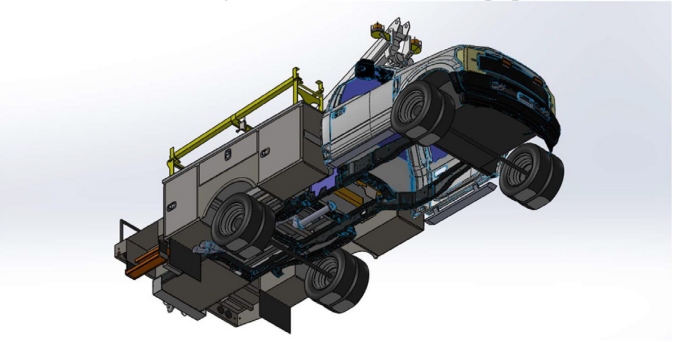

Figure 3. Bottom Isometric View: Complex CAD geometry of the utility truck with the boom equipment

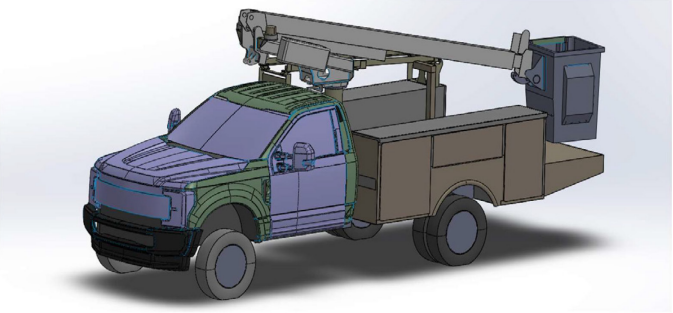

Figure 4. Simplified CAD geometry of the Utility Truck

In the imported geometry to SpaceClaim, a few components automatically rendered as transparent, which indicates the presence of unstitched edges, gaps between edges, and missing surfaces. This will create many errors while generating the mesh. Therefore, these need to be resolved before proceeding to mesh generation. The gaps between different patches in the geometry were closed by adding surface patches. The shrink wrap option in SpaceClaim was used to create a triangulated STL surface of the truck geometry.

The reverse engineering method was used to create the CAD definition of the geometry from the STL geometry of the truck. SpaceClaim is an integral part of ANSYS to clean up and repair the complex CAD model by recreating it using the "Auto Skin" command [15]. Unfortunately, numerous errors such as bad faces and extra edges occurred due to the quality of STL definition and the complexity of the original model, as shown in Figure 5. Therefore, the geometry is created from the STL definition using manual approach by using the “Skin Surface" in SpaceClaim. This function allows creating patches to the model until it turns solid without any gaps between the patches, as shown in Figure 6. Nevertheless, the model still was complex and cause errors during the mesh generation. So, the model was edited to simplify the complexity and smooth the surfaces before turning it into a solid model. Autodesk Meshmixer program [16] was used to clean up the model's surfaces and eliminate some of the complex areas. After the clean-up process, “Auto Skin” option in SpaceClaim was used to complete the final model without any errors, as shown in Figure 7.

In summary, the geometry preparation was done using the following steps in order: 1) initial simplification was done using SolidWorks, 2) fixing the gaps between patches was done using SpaceClaim, 3) creation of triangulated STL geometry was done using Shrink Wrap option in SpaceClaim, 4) simplification and smoothing of the STL geometry was carried out using AutoDesk MeshMixer, and 5) reverse engineering of the STL geometry was done using Auto Skin option in SapceClaim.

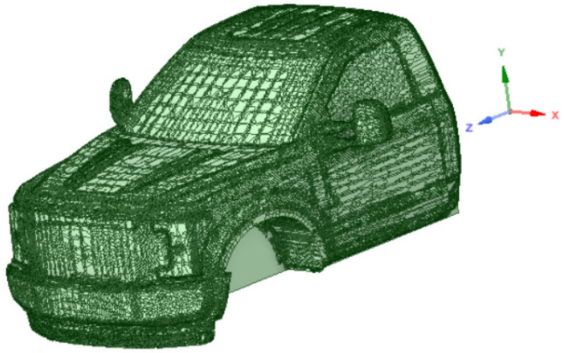

Figure 5. Complexity of the model in STL format

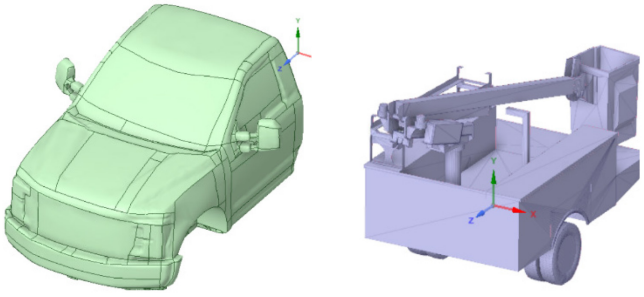

Figure 6. Skin Surface patched solid model

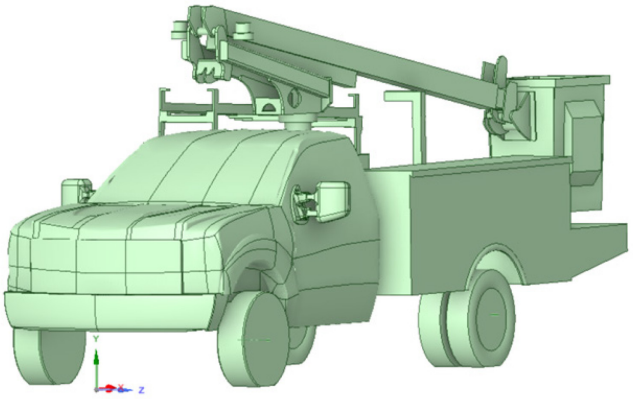

Figure 7: Final Solid CAD model of the utility truck

3.2 Numerical Modelling

Turbulence flow exhibits an unsteady behavior in complex geometry like a utility truck even when the steady state boundary condition is defined. This unsteadiness behavior can be resolved with the help of numerical simulations. Unfortunately, these extensive numerical simulations are often very time and memory consuming in complex flow. Thus, the unsteady Reynolds averaged Navier Stokes (URANS) approach is an alternative way to solve this problem. These URANS are very beneficial when the numerical simulations are used as a design and optimization tool. Frequently, the URANS simulation is implemented in the investigation of long-term periodical oscillations in a turbulent flow. The turbulent fluctuations of flow quantities are not determined in the URANS simulations, and thus, it assists to save computing time and computer memory.

With the usual notations, the incompressible unsteady Reynolds Averaged Navier Stokes equations (URANS) equations written as [17]

$$\frac{\partial \rho}{\partial t} + \frac{\partial (\rho u_i)}{\partial x_i} = 0 \tag{1}$$

$$\frac{\partial (\rho u_i)}{\partial t} + \frac{\partial (\rho u_i u_j)}{\partial x_j} = -\frac{\partial p}{\partial x_i} + \frac{\partial}{\partial x_j}\left[\mu\left(\frac{\partial u_i}{\partial x_j} + \frac{\partial u_j}{\partial x_i} - \frac{2}{3}\delta_{ij}\frac{\partial u_l}{\partial x_l}\right)\right] + \frac{\partial}{\partial x_j}\left(-\rho\overline{u_i' u_j'}\right) \tag{2}$$

The Reynolds stress appearing in the momentum equation can be written using the Boussinesq hypothesis as [17]

$$-\rho\overline{u_i' u_j'} = \mu_t\left(\frac{\partial u_i}{\partial x_j} + \frac{\partial u_j}{\partial x_i}\right) - \frac{2}{3}\left(\rho k + \mu_t \frac{\partial u_k}{\partial x_k}\right)\delta_{ij} \tag{3}$$

The eddy viscosity μ_t in the above equation is estimated using the two equations $k-\omega$ shear-stress transport (SST) turbulence model which is given by [17]

$$\mu_t = \frac{\rho k}{\omega}\frac{1}{\max\left[\frac{1}{\alpha^*}, \frac{SF_2}{a_1 \omega}\right]} \tag{4}$$

where S is the strain rate magnitude, $a_1 = 0.31$ and α^* is a coefficient which is defined as [17]

$$\alpha^* = \alpha_\infty^* \left(\frac{\alpha_0^* + Re_t/R_k}{1 + Re_t/R_k}\right) \tag{5}$$

where

$$Re_t = \frac{\rho k}{\omega \mu} \tag{6}$$

$$R_k = 6 \tag{7}$$

$$\alpha_0^* = \frac{\beta_i}{3}, \alpha_\infty^* = 1 \tag{8}$$

$$\beta_i = 0.072 \tag{9}$$

F_2 in equation 4 is given by

$$F_2 = tanh(\emptyset_2^2) \tag{10}$$

$$\emptyset_2 = \max\left[2\frac{\sqrt{k}}{0.09\omega y}, \frac{500\mu}{\rho y^2 \omega}\right] \tag{11}$$

where y is the distance to the next surface.

The advantage of choosing two equations shear-stress transport (SST) turbulence model in this paper is that it considers the transport of the principal turbulence shear stress in the near-wall region. Furthermore, it is widely used in vehicle aerodynamics and is efficient and accurate [18].

3.3 Validation of the URANS Model

The validation of the URANS model used in these simulations were achieved using the experimental data available for the airflow around the Ahmed body. The Ahmed body as shown in Figure 8, which was proposed by Ahmed et al. [11] features real vehicle flow field characteristics in three dimensions. The Ahmed body is a well-accepted benchmark case for both academic and industrial applications due to its geometric simplicity, while maintaining vehicle flow features.

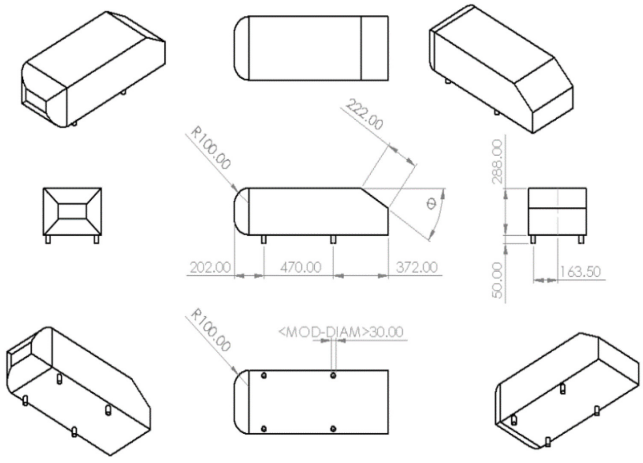

Figure 8: Geometry of the Ahmed Body

The geometry has a length of 1.044 meters with the ratio of the length, width, and height being 3.36: 1.37: 1. The middle of the body is a cuboid, and the edges of the front body are curved. There is a slant surface at the top rear whose angles range between 0º and 40º degrees. It also has four-cylindrical poles called stilts, attached to the bottom of the main body. The geometry of the Ahmed body with the rear slant angles of 25º and 35º and the meshes for the computational simulations are generated using the ANSYS Fluent software [19]. In this geometry, the origin of the coordinate system was placed at front end of Ahmed body, with $x = 0$ start of the model, $y = 0$ at the symmetric plane, and $z = 0$ at the ground plane. The mesh used for the simulation was composed of around 8 million elements for both the slant angles as represented in Figure 9. As shown in the figure, we have used three different regions for mesh refinement to capture the wake and the flow around the body with a better accuracy.

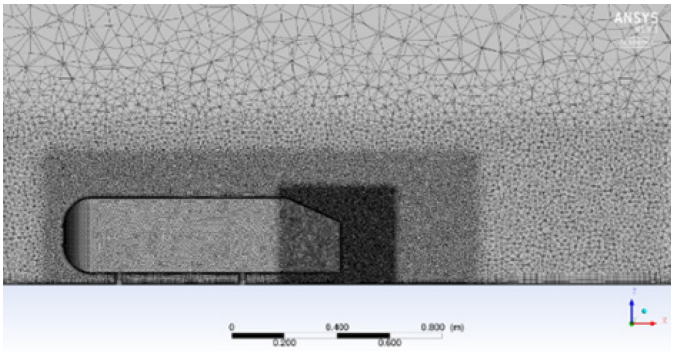

(a) 25 Degree

(b) 35 Degree

Figure 9. Near mesh of the Ahmed body

In these simulations, the velocity inlet was taken as 40 m/s. Since the flow speed less than Mach number 0.3, it was assumed that flow is incompressible, and the density was set to a constant value. For the solution of the governing equation, the time derivatives were discretized using first order and the spatial derivatives in the continuity and momentum equations were discretized using a second-order upwind method. A least-squares cell-based method was applied in the estimation of the gradients of the flow variables. A coupled numerical approach was used for the solution of the continuity and the momentum equations. Finally, a first-order upwind technique was applied for the solution of the turbulent kinetic energy and specific dissipation rate equations for the k-ω SST model.

For the boundary conditions, a stationary wall with no-slip boundary condition was specified to simulate the rigid parts such as the Ahmed body, pegs, and the computational domain ground. The boundary condition for the computational domain sidewalls and the top surface was defined as a slip boundary condition. At inlet the velocity was set as 40 m/s and the outlet, the gage pressure was set as 0 Pa.

The summary of the results from the simulations are tabulated in Table 1. It can be seen from the table that the computational results are in good agreement with the experimental data and results from other simulations. This validates the models used for the air flow simulation around the Ahmed body, and applicability of these models for simulation of vehicle aerodynamics.

Table 1: Comparison of the predicted drag coefficient with experimental data and other published data for both slant angles

Slant angle	35º		25º	
	Without stilts	With stilts	Without stilts	With stilts
Experimental data [11]	X	0.260	X	0.285
Our simulation	0.282	0.3096	0.2958	0.3233
Simulation data [20]	0.2895	0.3133	0.3074	X

4. CFD SIMULATIONS AND RESULTS OF THE UTILITY TRUCK

A rectangular block around the utility truck was selected as the computational domain as shown in Figure 10. The computational domain was divided into six parts: two side walls, top, ground, inlet, and outlet. The length of the computational domain was taken as 75 m, width was taken as 44 m and the height was taken as 21 m.

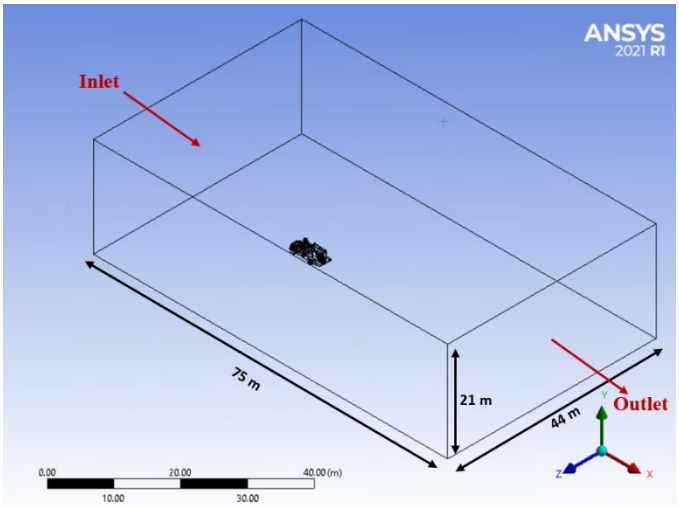

Figure 10. Computational domain with the Utility Truck

The computational domain mesh was discretized using a generalized mesh topology, and the boundary layer mesh was applied around the utility truck model, as shown in Figure 11. The generated mesh for the zero-degree side slip angle consisted of 10,709,407 elements and 4,057,693 nodes. Zoomed-in views of the mesh at different locations on the boundary surface and a cutting plane are shown in Figure 12. These figures also show the boundary layer mesh used for the simulations. To mimic different side slip angles, the utility truck was rotated inside the computational domain, which resulted in a slightly different number of elements and nodes for different side slip angles. Thus, the resulting mesh will have a different elements and nodes at various side slip angles.

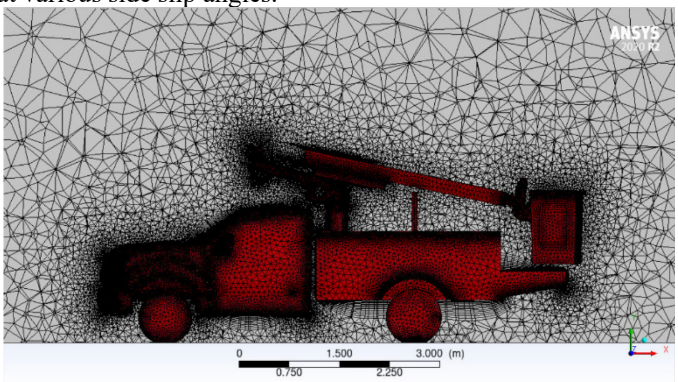

Figure 11. Near mesh of the Utility Truck

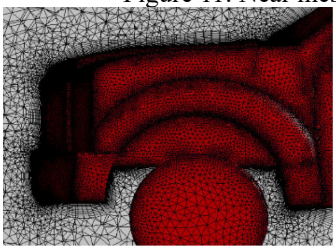

(a) Front bumper side and cabin

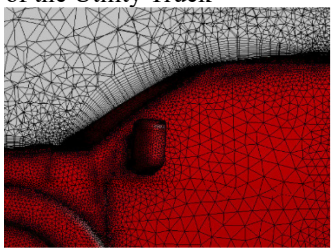

(b) Mirror

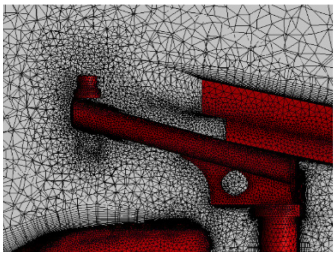

(c) The boom equipment

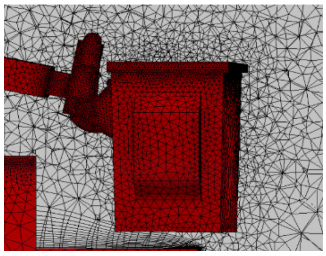

(d) Bucket

Figure 12. Zoomed-in view of the mesh

Unsteady CFD simulations were performed using a step size pf 0.003 seconds and each simulation was run for 1000-time steps. The residuals and the drag-plot were checked to make sure that the solution was stabilized, and the force and moment coefficients reached asymptotic values. The validated numerical aerodynamic model with boundary conditions used for the Ahmed body, was used to simulate wind flow around the utility truck. Computational simulations were carried out for side slip angles of 0 to 35 in steps of 5 degrees. The static pressure distribution on the utility truck for these side slip angles are shown in Figure 13.

In these simulations, the static pressure distribution of the front and left sides of the truck ranged from -4036.4 to 999.39 Pa. The negative pressure areas were primarily at the top and right-side surfaces of the utility truck, while other areas directly facing the wind had positive pressure. The positive area at the cabin front and the boom equipment gradually shifts towards the left side due to the increased side slip angle. Thus, it becomes more prominent, leading to increased side force. Furthermore, the increased positive pressure area at the front of the cabin and the boom equipment causes the aerodynamic drag force on the utility truck to increase, which can be seen from the static pressure distribution.

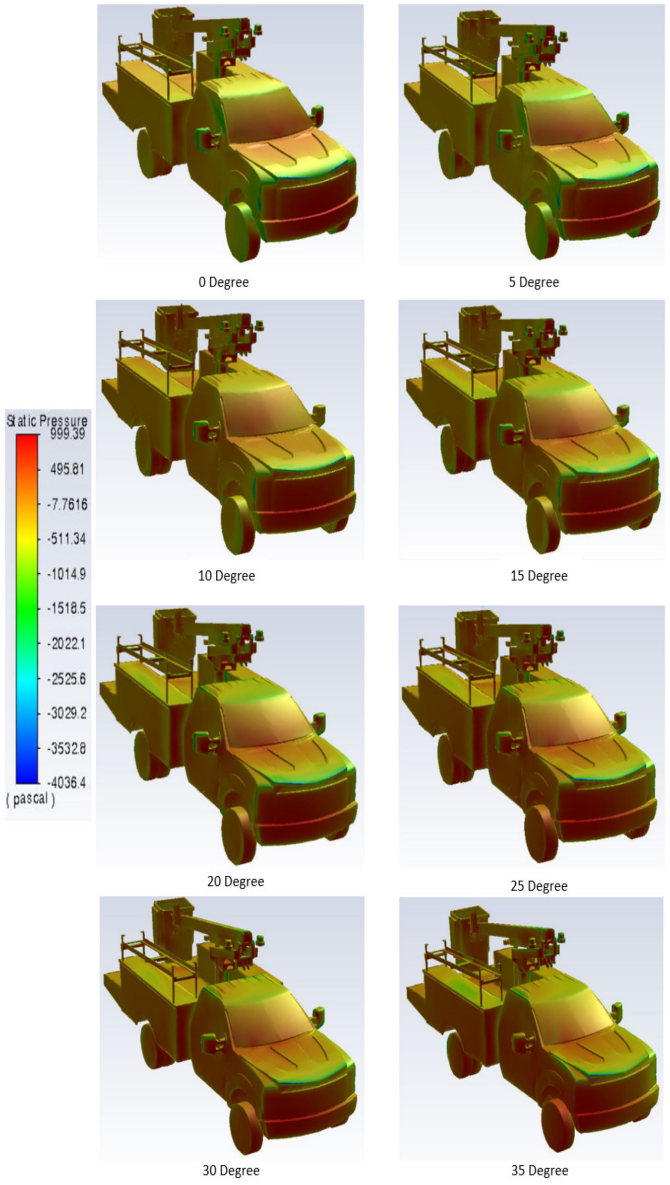

Figure 13. Static pressure distribution on the utility truck

The velocity contours around the utility truck at the 10^o side slip angle on the symmetry plane and a few streamlines around the truck are shown in Figure 14 and Figure 15 respectively. These figures show the complex separated flow pattern around the utility truck. The air, when it reaches the end of the trailer and at the very beginning of the bucket, gets separated from the surfaces and causes a swirling flow behind the bucket. Furthermore, the air undercarriage of the trailer gets separated from the trailing end surface, which generates a small swirl underneath as represented in Figure 15.

A low-pressure region is created behind the bucket when the separation of the air occurs, which increases the drag force acting on the truck, Thus, it is advisable to put the bucket at a different angle, i.e., in the horizontal direction, to reduce the low-pressure region on the trailer backside of the truck.

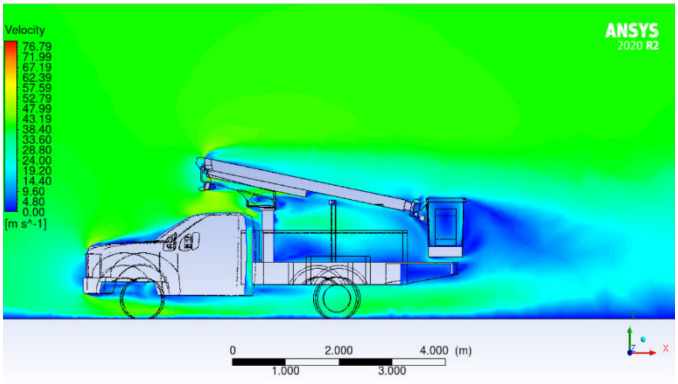

Figure 14. Velocity contours at the symmetry plane around the utility truck at 10^o side slip angle

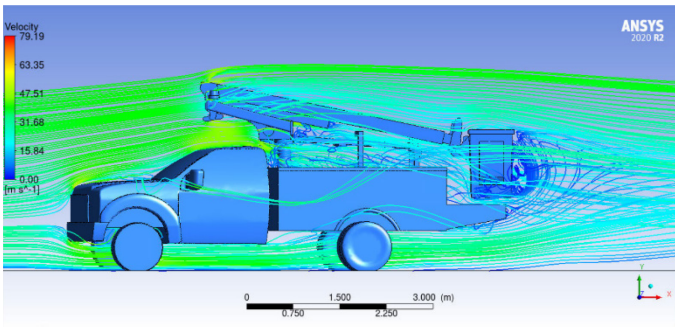

Figure 15. Velocity streamlines at the symmetry plane around the utility truck at 10^o side slip angle

4.1 Aerodynamic Coefficients

When aerodynamic forces interact with the truck, it generates drag, lift, and lateral forces, and pitch, roll and yaw moments. The aerodynamic forces and moments are typically written in terms of the non-dimensional force and moment coefficients and the reference conditions defined as follows [21]

$$D_A = \frac{1}{2} C_D \, \rho A V^2 \quad (12)$$

$$L_A = \frac{1}{2} C_L \, \rho A V^2 \quad (13)$$

$$S_A = \frac{1}{2} C_S \, \rho A V^2 \quad (14)$$

$$PM = \frac{1}{2} C_{PM} \, \rho A V^2 L \quad (15)$$

$$RM = \frac{1}{2} C_{RM} \, \rho A V^2 L \quad (16)$$

$$YM = \frac{1}{2} C_{YM} \, \rho A V^2 L \quad (17)$$

where D_A is the drag force, L_A is the lift force, S_A is the side force, PM is the pitching moment, RM is the rolling moment, YM is the yawing moment, C_D is the drag coefficient, C_L is the lift coefficient, C_S is the side force coefficient, C_{PM} is the pitching moment coefficient, C_{RM} is the rolling moment coefficient, C_{YM} is the yawing moment coefficient, ρ is the density of the air, A is the frontal area of the truck, V is the total velocity of vehicle speed and wind speed, and L is the reference length.

In these calculations, the reference area is taken as 5.334077 m^2, reference length is taken as 1 m, reference velocity is taken as 40 m/s, and reference density is taken as 1.225 kg/m^3. In this truck geometry, the origin of the coordinate system is placed according to the SAE aerodynamic reference point [22] as a wheelbase mid-point along the intersection of vehicle plane of symmetry and at the ground, as shown in Figure 16. For the calculation of the moments, the moment center is taken as the origin of the coordinate system. These forces and moments are calculated by CFD simulations for 8 side slip angles. All the results of aerodynamic forces and moments are shown in Figures 17 and 18.

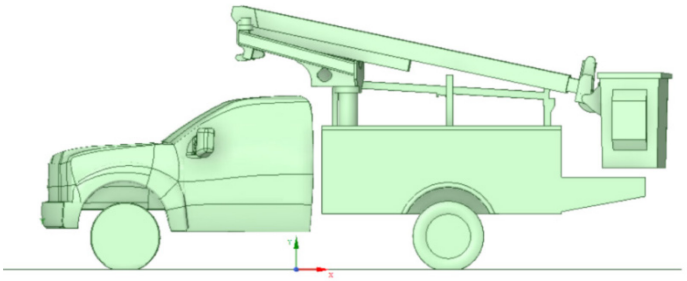

Figure 16. Origin of the coordinate system

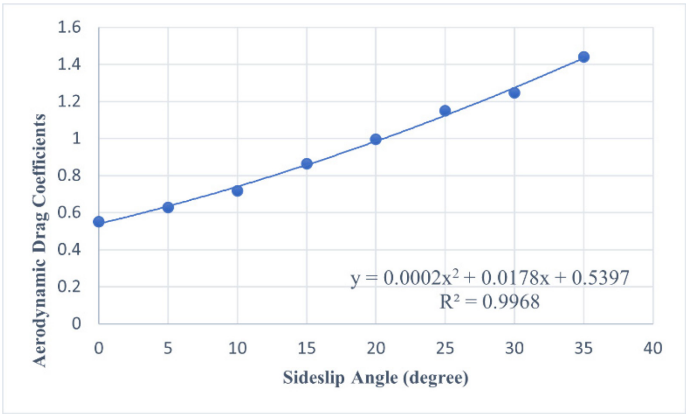

(a) Aerodynamic drag coefficients

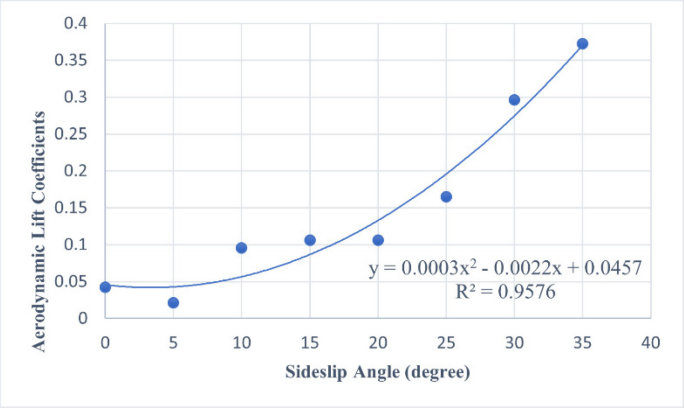

(b) Aerodynamic lift coefficients

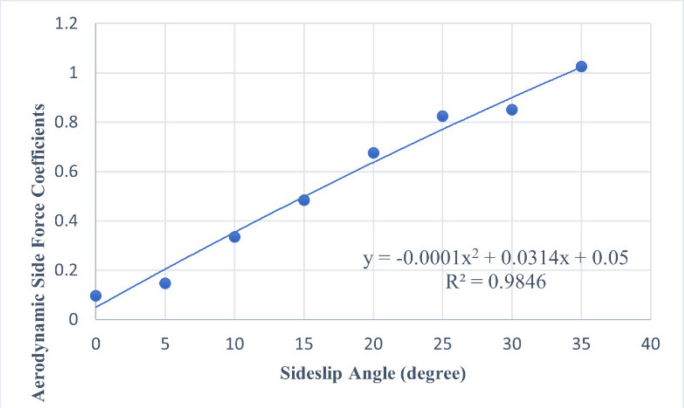

(c) Aerodynamic side force coefficients

Figure 17. Variation of force coefficients for different side slip angles

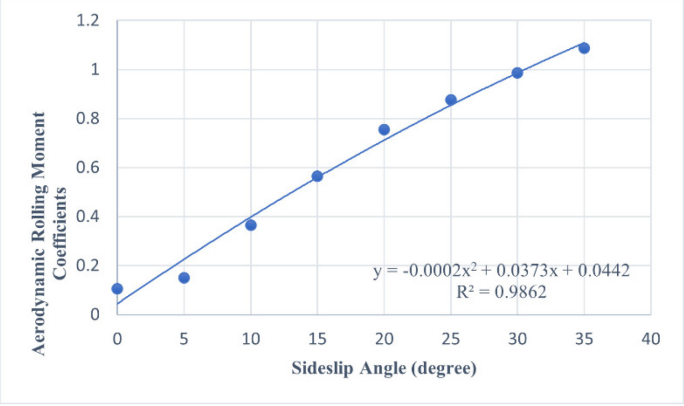

(a) Aerodynamic rolling moment coefficients

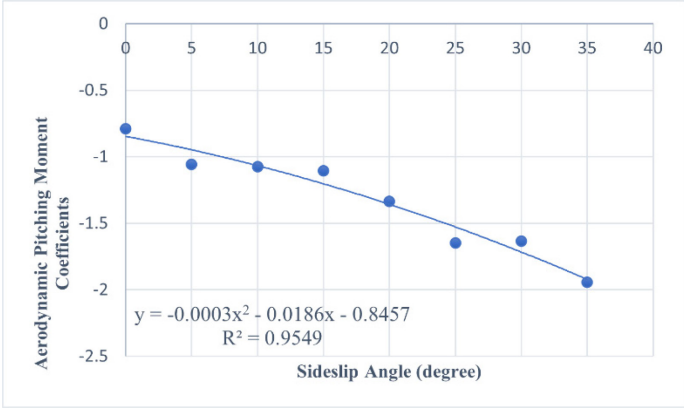

(b) Aerodynamic pitching moment coefficients

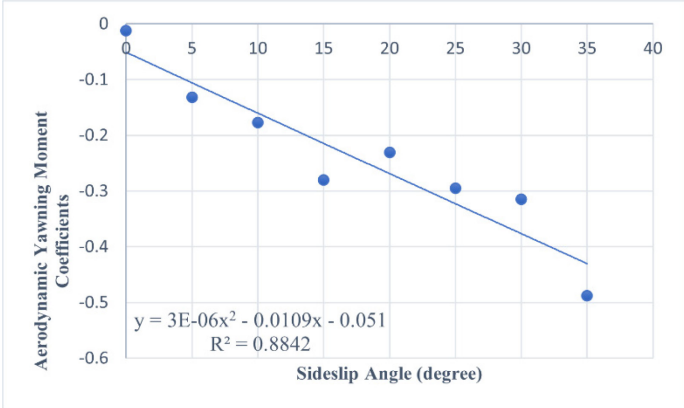

(c) Aerodynamic yawing moment coefficients

Figure 18. Variation of moment coefficients for different side slip angles

As shown in Figures 17 and 18, the force and moment coefficients vary with the side slip angles, and thus, these coefficients are the functions of the side slip angle. All these aerodynamic coefficients are fitted with the quadratic polynomials, and the fitted curves are written as follows

$$C_D = 0.0002\alpha^2 + 0.0178\alpha + 0.5397 \quad (18)$$
$$C_L = 0.0003\alpha^2 - 0.0022\alpha + 0.0457 \quad (19)$$
$$C_S = -0.0001\alpha^2 + 0.0314\alpha + 0.05 \quad (20)$$
$$C_{RM} = 0.0002\alpha^2 + 0.0178\alpha + 0.5397 \quad (21)$$
$$C_{YM} = (3E-06)\alpha^2 - 0.0109\alpha - 0.051 \quad (22)$$
$$C_{PM} = -0.0003\alpha^2 - 0.0186\alpha - 0.8457 \quad (23)$$

where α is the side slip angle in degrees. The R^2 value of the fitted polynomials were all above 0.9.

The CFD simulations provide the aerodynamic drag coefficient values in the range of 0.55 – 1.45 for the range of $0^o - 35^0$ of side slip angle. The value of aerodynamic drag coefficient for a heavy-duty truck at zero side slip angle without the boom equipment is 0.45 [21]. It can be inferred that the value of drag coefficient for the utility truck with the boom equipment will be higher since the boom equipment adds more reference

frontal area and more complex flow features. Additionally, the drag created by the wind impinging on the front of the truck, and the large momentum changes of the wind hitting the trailer adds another larger drag component in crosswind conditions.

Lift force is totally dependent on the overall shape of the vehicle and the pressure distribution underneath and top of the vehicle. Lift coefficients normally fall in the range of 0.3 to 0.5 for the passenger cars at zero wind angle [23], which shows the good agreement of the CFD simulations of the utility truck. But under crosswind conditions, the coefficient value may increase dramatically, reaching values one or more [24]. This phenomenon is spotted in Figure 19, which compares the static pressure distribution under neath of the utility truck. It can be seen from the figure that the pressure acting underneath the vehicle is much higher for 35 degrees side slip angle as compared to zero-degree side slip angle. This causes higher lift for higher side slip angle.

It is reported in the literature that the side force coefficient for automobiles is zero at zero relative wind angle, and it grows nearly linearly with the angle for the first 20 to 40 degrees from zero to one [21]. Similar behavior is also noted in the current simulation and the CFD simulations predicted linearity in the side force coefficients.

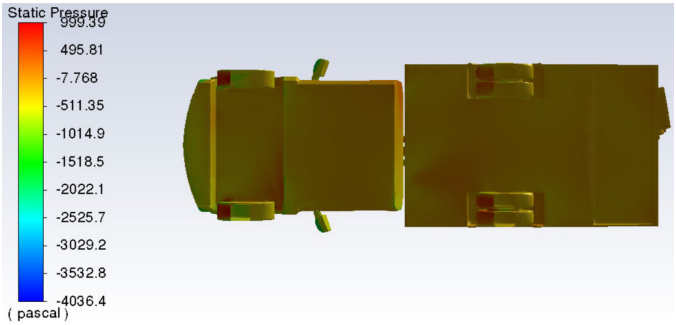

(a) Zero degree

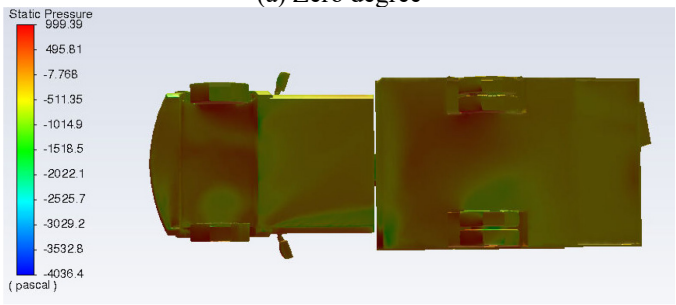

(b) 35 degrees

Figure 19. Comparison of static pressure surface distribution underneath the truck for different side slip angles

5. CONCLUSIONS

In conclusion, CFD simulations were used to investigate the aerodynamics of the utility truck with the boom equipment. The CAD geometry definition of the utility truck with the boom equipment contained much more information than needed for the simulation and was not a water-tight geometry needed for simulations. This geometry was fixed and prepared to run the CFD simulations with the help of SolidWorks, SpaceClaim and Autodesk MeshMixer software. The incompressible unsteady Reynolds Averaged Navier Stokes (URANS) model used for the analysis was validated with the well-acknowledged Ahmed body, which is the benchmark test case used by the CFD community for the aerodynamic validation of automobiles. This validated aerodynamic model was used to study the aerodynamic characteristics of the utility truck. The predicted aerodynamic force and moment coefficients are comparable to the coefficient values of the pick-up truck. Finally, all these aerodynamic coefficients were expressed as quadratic functions with the slide slip angles as a variable using curve fitting.

ACKNOWLEDGEMENTS

This research work is supported by NSF award S&AS-1849264. The authors gratefully acknowledge the resources provided by the University of Alabama at Birmingham IT-Research Computing group for high performance computing support (HPC) and CPU time on the Cheaha compute cluster. We would like to express our gratefulness to Altec Inc., our research partner for providing CAD geometry of the utility truck and required data for the research analysis, which aided us to progress in our research.

REFERENCES

[1] National Weather Service, NOAA (2016). Appendix: Fujita Scale (or F Scale) of Tornado Damage Intensity. URL: https://www.weather.gov/oun/tornadodata-okc-appendix (Accessed: 22 November 2016).

[2] National Weather Service, NOAA (2016). Saffir-Simpson Hurricane Wind Scale. URL: https://www.nhc.noaa.gov/aboutsshws.php (Accessed: 22 November 2016).

[3] "Freight facts and figures 2015, US department of transportation, bureau of transportation statistics,". URL: http://www.princeton.edu/~alaink/Orf467F16/FHWA2201FreightFactsF_complete.pdf/.

[4] William Y, Oraby W and Metwally S. Analysis of vehicle lateral dynamics due to variable wind gusts. SAE technical paper 2014-01-2449, 2014. doi: https://doi.org/10.4271/2014-01-2449.

[5] Hussain K, Rahnejat H and Hegazy S. Transient vehicle handling analysis with aerodynamic interactions. Proc IMechE, Part K: J Multi-body Dynamics 2007; 221:21–32. doi: https://doi.org/10.1243/1464419JMBD41.

[6] Dominy RG and Richardson S. The aerodynamic characteristics of a WRC rally car at high slip angles. SAE technical paper 2004-01-3508, 2004. doi: https://doi.org/10.4271/2004-01-3508.

[7] Tsubokura M, Nakashima T, and Ikenaga T. HPC-LES for the prediction of unsteady aerodynamic forces on a vehicle in a gusty crossflow condition. SAE technical paper 2008-01-300, 2008. doi: https://doi.org/10.4271/2008-01-3001.

[8] Walmart Inc., "Walmart Debuts Futuristic Truck,". URL: https://corporate.walmart.com/newsroom/2014/03/26/walmart-debuts-futuristic-truck.

[9] Department of Energy, "SuperTruck Making Leaps in Fuel Efficiency," URL: http://energy.gov/eere/articles/supertruck-making-leaps-fuel-efficiency.

[10] McAuliffe, B.R. and Wall, A.S., "Aerodynamic Performance of Flat-Panel Boat-Tails and Their Interactive Benefits with Side-

Skirts," SAE International Journal of Commercial Vehicles 9:70–82, 2016, doi:10.4271/2016-01-8015.
[11] S. R. Ahmed, G. Ramm, and G. Faltin. Some salient features of the time averaged ground vehicle wake. SAE Paper 840300, 1984. doi: https://doi.org/10.4271/840300.
[12] Altec Industries, Inc. URL: https://www.altec.com/.
[13] BIOVIA, Dassault Systèmes, Solidworks 2021 SP2.0, San Diego: Dassault Systèmes, 2021.
[14] Ansys® SpaceClaim, Release 2020R2.
[15] Data Sheet: "SpaceClaim for Reverse Engineering, Edit Without Constraints to Perfect Each Feature". URL: http://www.spaceclaim.com/files/documents/SPC_Rev%20Engineering%20DS-Web.pdf.
[16] Autodesk Meshmixer: state-of-the-art software for working with triangle meshes, Release 3.5, 2018.
[17] ANSYS Fluent Theory Guide, 2020R1, January 2020.
[18] Paul Schreier, Modelling: Aerodynamics, turbulent times, Scientific computing world, June/July 2010.
[19] Ansys® Fluent, Release 2020R2.
[20] E Guilmineau. Computational study of flow around a simplified car body. J Wind Eng Ind Aerodyn 2008;96(6):1207–17. doi: https://doi.org/10.1016/j.jweia.2007.06.041.
[21] Gillespie, Thomas D. 1992. Fundamentals of Vehicle Dynamics. Premiere Series Books. Warrendale: SAE International.
[22] SAE J1939-21:2011. Surface vehicle recommended practice. The engineering society for advancing mobility land sea air and space.
[23] Aerodynamics of Road Vehicles, Wolf-Heinrich Hucho, ed., Butterworths, London, 1 987, 566 p.
[24] Hogue, J.R., "Aerodynamics of Six Passenger Vehicles Obtained from Full Scale Wind Tunnel Tests," SAE Paper No. 800142, 1980, 17 p. doi: https://doi.org/10.4271/800142